Neuroendocrinology

Neuroendocrinology , DOI: 10.1159/000517087
Received: March 29, 2021
Accepted: April 30, 2021
Published online: May 7, 2021

Molecular identification and cellular localisation of a corticotropin-releasing hormone type neuropeptide in an echinoderm

Cai W, Egertová M, Zampronio CG, Jones AM, Elphick MR

ISSN: 0028-3835 (Print), eISSN: 1423-0194 (Online)
https://www.karger.com/NEN
Neuroendocrinology

Molecular identification and cellular localisation of a corticotropin-releasing hormone type neuropeptide in an echinoderm

Weigang Cai[a], Michaela Egertová[a], Cleidiane G. Zampronio[b],
Alexandra M. Jones[b], Maurice R. Elphick[a]

[a] Queen Mary University of London, School of Biological & Chemical Sciences, Mile End Road, London E1 4NS, UK
[b] School of Life Sciences and Proteomics Research Technology Platform, University of Warwick, Coventry, CV4 7AL, UK

Short Title: CRH-type neuropeptide in an echinoderm

Corresponding Author:
Prof. Maurice R. Elphick
School of Biological & Chemical Sciences
Queen Mary University of London
London E1 4NS, UK.
Tel: +44(0) 20 7882 6664
Fax: +44(0) 20 7882 7732;
E-mail: m.r.elphick@qmul.ac.uk

Number of Tables: 1 supplemental table
Number of Figures: 9 figures and 4 supplemental figures.
Word count: 5795
Keywords: *Asterias rubens*, corticotropin-releasing hormone, starfish, neuropeptide, deuterostome.

Abstract

Background: Corticotropin-releasing hormone (CRH) mediates physiological responses to stressors in mammals by triggering pituitary secretion of adrenocorticotropic hormone, which stimulates adrenal release of cortisol. CRH belongs to a family of related neuropeptides that include sauvagine, urotensin-I and urocortins in vertebrates and the diuretic hormone DH44 in insects, indicating that the evolutionary origin of this neuropeptide family can be traced to the common ancestor of the Bilateria. However, little is known about CRH-type neuropeptides in deuterostome invertebrates. ***Methods:*** Here we used mass spectrometry, mRNA *in situ* hybridization and immunohistochemistry to investigate the structure and expression of a CRH-type neuropeptide (ArCRH) in the starfish *Asterias rubens* (phylum Echinodermata). ***Results:*** ArCRH is a 40-residue peptide with N-terminal pyroglutamylation and C-terminal amidation and it has a widespread pattern of expression in *A. rubens*. In the central nervous system comprising the circumoral nerve ring and five radial nerve cords, ArCRH-expressing cells and fibres were revealed in both the ectoneural region and the hyponeural region, which contains the cell bodies of motoneurons. Accordingly, ArCRH-immunoreactivity was detected in innervation of the ampulla and podium of locomotory organs (tube feet), and ArCRH is the first neuropeptide to be identified as a marker for nerve fibres located in the muscle layer of these organs. ArCRH-immunoreactivity was also revealed in protractile organs that mediate gas exchange (papulae), the apical muscle and the digestive system. ***Conclusions:*** Our findings provide the first insights into CRH-type neuropeptide expression and function in the unique context of the pentaradially symmetrical body plan of an echinoderm.

Introduction

The existence of a hypothalamic neurohormone that stimulates pituitary secretion of adrenocorticotropic hormone (ACTH) was first postulated in the 1950s [1-3]. However, it was not until 1981 that this corticotropin-releasing hormone (CRH) was identified as an amidated 41-residue peptide [4], which is derived from the C-terminal region of a 196-residue precursor protein [5, 6]. Sequencing of CRH revealed that it is a homolog of sauvagine and urotensin-I, vasoactive peptides isolated from the skin of the frog *Phyllomedusa sauvagii* [7] and the urophysis of teleost fish, respectively [8, 9]. Thus, a family of related bioactive peptides were discovered in vertebrates and more recently genes encoding CRH/sauvagine/urotensin-1-like peptides named urocortin 1 (UCN1), urocortin 2 (UCN2) and urocortin 3 (UCN3) were identified in humans and other mammals [10-12]. CRH/UCN-type peptides exert effects via two G-protein coupled receptors in humans known as CRHR1 and CRHR2, with CRHR1 selectively activated by CRH and UCN1 and CRHR2 non-selectively activated by all four peptides [13-15]. Furthermore, investigation of the phylogenetic distribution of CRH/UCN-type neuropeptide signalling in vertebrates by comparative analysis of genome sequence data indicates that a common ancestor of vertebrates would have had one gene encoding a CRH/UCN1 type neuropeptide, one gene encoding a UCN2/UCN3-type neuropeptide and one gene encoding a receptor for these two neuropeptides. Then genome duplications followed by gene loss gave rise to variety in the complement of genes encoding CRH/UCN-type precursors and receptors in different vertebrate lineages [15, 16]. Genes encoding CRH-type precursors and CRH-type receptors have also been identified in the invertebrate chordates *Ciona intestinalis* (sub-phylum Urochordata) and *Branchiostoma floridae* (sub-phylum Cephalochordata), providing insights into the pre-vertebrate origins of CRH-type neuropeptide signalling in the phylum Chordata [17, 18].

A key advance in our knowledge and understanding of the evolution of CRH/UCN-type signalling was made with the discovery of a 44-residue diuretic hormone (DH44) in the insect *Manduca sexta* that shares sequence similarity with CRH and UCNs [19]. Subsequently, DH44-type peptides were identified in other insects and further evidence that DH44 is a homolog of CRH/urocortin-type peptides in vertebrates was obtained with the identification of DH44 receptors as homologs of vertebrate CRH/UCN-type receptors [20-22]. Thus, the discovery of the DH44 signalling system in insects revealed that the evolutionary origin of CRH/UCN-type signalling can be traced back to the urbilaterian common ancestor of protostome invertebrates (e.g. insects) and vertebrates. Accordingly, precursors of DH44-like neuropeptides have also been identified in other protostomes, which include egg-laying hormone in gastropod molluscs [18, 23].

Important insights into the evolution and comparative physiology of neuropeptide signalling systems have been obtained recently from studies on non-chordate deuterostomes (echinoderms and hemichordates), which occupy an 'intermediate' phylogenetic position with respect to chordates and protostomes [24]. In particular, the starfish *Asterias rubens* (class Asteroidea) has been used extensively as an experimental system for molecular and functional characterisation neuropeptide signalling systems [25]. For example, molecular characterisation of neuropeptide signalling systems in *A. rubens* has provided key insights for reconstruction of the evolutionary history of neuropeptide-S (NPS)/crustacean cardioactive peptide (CCAP)-type [26, 27], gonadotropin-releasing hormone (GnRH)/corazonin-type [28, 29] and prolactin-releasing peptide (PrRP)/short neuropeptide-F (sNPF)-type neuropeptide signalling [30]. Furthermore, functional characterisation of neuropeptides in *A. rubens* has provided new insights into the comparative physiology of, for example, GnRH/corazonin-type [31], calcitonin-type [32], vasopressin/oxytocin-type [33] and somatostatin-type [34] neuropeptides.

Analysis of *A. rubens* neural transcriptome sequence data recently enabled identification of a transcript encoding the first precursor of a CRH-type peptide to be discovered in an echinoderm, which is referred to as ArCRH [35]. The discovery of this precursor provides an opportunity for characterisation of a CRH-type peptide in an echinoderm. Accordingly, here we report use of mass spectrometry to determine the structure of the CRH-like neuropeptide derived from the ArCRH precursor protein. Furthermore, we report use of mRNA *in situ* hybridisation and immunohistochemistry, employing novel antibodies to ArCRH, to enable a detailed analysis of ArCRH expression in *A. rubens*.

Materials and Methods

Animals

Specimens of the starfish *A. rubens* Linnaeus 1758, (diameter >4 cm) were collected at low tide from the Thanet coast, Kent, UK, or were obtained from a fisherman based at Whitstable, Kent, UK. The starfish were maintained in an aquarium with circulating artificial seawater at ~12°C and were fed weekly on mussels (*Mytilus edulis*). Smaller juvenile starfish (diameter 0.5 – 1.5 cm) were collected at the University of Gothenberg Sven Lovén Centre for Marine Infrastructure (Kristineberg, Sweden) and fixed in the Bouin's solution.

Determination of the structure of ArCRH and comparison of its sequence with CRH and CRH-related peptides in other taxa

A transcript encoding an *A. rubens* CRH-type precursor (ArCRHP) was identified previously based on analysis of neural transcriptome sequence data [35] and a cDNA encoding ArCRHP has been cloned and sequenced [36]. The predicted CRH-type peptide derived from ArCRHP is a 40-residue peptide with an amidated C-terminus. To determine if this predicted structure of ArCRH is correct, extracts of radial nerve cords from *A. rubens* were prepared and analysed using mass spectrometry (Nano-LC-ESI-MS/MS), employing methods described in detail previously [37, 32]. Briefly, extracts were fractionated by reversed phase chromatography on an Ultimate 3000 RSLCnano system (Dionex) and then injected directly via a Triversa Nanomate nanospray source (Advion Biosciences, NY) into a Thermo Orbitrap Fusion (Q-OT-qIT, Thermo Scientific) mass spectrometer. Data analysis was performed using Proteome Discoverer 2.2 (Thermo Fisher Scientific) with an ion mass tolerance of 0.050 Da and a parent ion tolerance of 10.0 ppm. C-terminal amidation and N-terminal pyroglutamylation were specified as potential post-translational modifications. Furthermore, differentiating the presence of isobaric residues (leucine and isoleucine) and near isobaric residues (lysine and glutamine) in peptide fragments was enabled by the availability of the ArCRH sequence predicted from cDNA sequencing. In addition, synthetic ArCRH with the predicted structure pQGLSVSPIFPIQRIRLNAIERDRQDQVDQAEANQGLFQIA-NH_2 was synthesized and purified (>95%) by Peptide Protein Research Ltd (Fareham, Hampshire, UK) (Supplemental Fig. 1) and then also analysed using mass spectrometry to enable comparison of spectra with those obtained from analysis of radial nerve cord extracts. Having determined the structure of the mature ArCRH peptide, its sequence was aligned with CRH and CRH-related peptides from other species using the Clustal Omega mutiple sequence alignment program (https://www.ebi.ac.uk/Tools/msa/clustalo/).

Localization of ArCRHP expression in A. rubens using mRNA in situ hybridization

Digoxigenin-labelled RNA antisense probes complementary to ArCRHP transcripts and corresponding sense probes were synthesized, as reported previously [36]. The methods employed for visualization of ArCRHP expression in sections of the arms, central disk or whole-body of *A. rubens* were the same as those reported previously for analysis of the expression of the calcitonin-type precursor ArCTP [32], the relaxin-type precursor ArRGPP [37], the gonadotropin-releasing hormone type precursor ArGnRHP and the corazonin-type precursor ArCRZP [31], the pedal peptide-type precursor ArPPLNP1 [38] and somatostatin-type precursor ArSSP2 [34].

Production and characterization of a rabbit antiserum to the C-terminal region of ArCRH

To generate a rabbit antiserum against ArCRH (pQGLSVSPIFPIQRIRLNAIERDRQDQVDQAEAN QGLFQIA-NH_2), a peptide containing the C-terminal 10 amino acids of ArCRH (KEANQGLFQIA-NH_2) was synthesized and purified (>95%) by Peptide Protein Research Ltd (Fareham, Hampshire, UK) and then used as a peptide antigen (Supplemental Fig. 2). The N-terminal lysine residue was incorporated in the antigen peptide to provide a reactive site for conjugation with a carrier protein (porcine thyroglobulin; Sigma Aldrich). The conjugate of the antigen peptide and carrier protein was prepared by using 5% glutaraldehyde in phosphate buffer (PB, 0.1 M, pH 7.2) as a coupling reagent [39]. Then the solution was dialysed in distilled water to remove glutaraldehyde and any uncoupled peptide and then was divided into aliquots containing approximately 50 nmol conjugated antigen in each tube. Antiserum production in a male rabbit was carried out by Charles River Ltd (Margate, UK; project code number 17582) using the same immunization and bleeding protocol reported previously for generation of antisera to ArPPLN1b and ArCT [38, 32]. To assess the presence and titre of antibodies to the antigen peptide, pre-immune serum and antiserum from the final bleed was analysed using an enzyme-linked immunosorbent assay (ELISA), employing use of protocols similar to those reported previously for antisera to ArPPLN1b and ArCT [38, 32].

Immunohistochemical localization of ArCRH in A. rubens

The methods employed for immunohistochemical localization of ArCRH in *A. rubens* were the same as those reported previously for ArPPLN1b and ArCT [38, 32], but with the ArCRH antiserum being used at a dilution of 1:32,000.

RESULTS

Determination of the structure of the A. rubens CRH-type neuropeptide ArCRH and comparison with the sequences of CRH and CRH-related peptides in other taxa.

A cDNA encoding the ArCRH precursor (ArCRHP) has been cloned and sequenced [36], confirming a previously reported transcript sequence obtained from analysis of *A. rubens* neural transcriptome sequence data [35] (GenBank accession number KT601710.1). ArCRHP is a 130-residue protein comprising a predicted 28-residue N-terminal signal peptide (residues 1-28) followed by a pro-peptide, which includes a putative 41-residue CRH-like peptide sequence (QGLSVSPIFPIQRIRLNAIERDRQDQVDQAEANQGLFQIAG, residues 87-127) that is bounded by putative dibasic/tribasic cleavage sites N-terminally and C-terminally (Fig. 1a). The N-terminal glutamine (Q) and C-terminal glycine (G) residues of the 41-residue peptide are noteworthy as potential substrates for post-translational pyroglutamylation (pQ) and amidation (NH_2), respectively. Therefore, the predicted mature structure of ArCRH is pQGLSVSPIFPIQRIRLNAIERDRQDQVDQAEANQGLFQIA-NH_2.

To determine the mature structure of ArCRH, mass spectrometric methods were employed. To facilitate this a synthetic peptide with the predicted structure of ArCRH was analysed in parallel with analysis of *A. rubens* radial nerve cord extracts. Synthetic ArCRH was detected with a monoisotopic mass of m/z 1129.85 (4+) (Supplemental Fig. 3a) and with a deconvoluted molecular mass of 4515.38 based on the monoisotopic peak (not shown), which is consistent with the expected monoisotopic mass for the 40-residue ArCRH peptide with an N-terminal pyroglutamate residue and C-terminal amide group. Analysis of extracts of *A. rubens* radial nerve cords (which had not been treated with trypsin or the reducing agent dithiothreitol (DTT)) revealed the presence of two fragments of ArCRH: pQGLSVSPIFP [monoisotopic mass of 514.27 m/z (2+)] and SVSPIFPIQRIRLNAIERDRQDQVDQAEANQGLFQIA-NH_2 [monoisotopic mass of 847.85 m/z (5+)] (Fig. 1b; Supplemental Fig. 3b,c). Analysis of radial nerve cord extracts that had been treated with trypsin, but without DTT, revealed two peptide fragments of ArCRH, pQGLSVSPIFPIQR and DRQDQVDQAEANQGLFQIA-NH_2, with monoisotopic masses of 712.89 m/z (2+) and 715.68 m/z (3+), respectively (Fig. 1b; Supplemental Fig. 3d,e). In summary, the mass spectrometric analysis of *A. rubens* radial nerve cord extracts under different experimental conditions confirmed the predicted sequence of ArCRH, with an N-terminal pyroglutamate and a C-terminal amide identified as post-translational modifications (Fig. 1b).

Having determined the structure of ArCRH, we compared it with the sequences of CRH and CRH-related peptides in other taxa, as shown in the alignment in Fig. 1c. As a 40-residue peptide ArCRH has a typical length for a CRH-type peptide as illustrated by the peptides included in the alignment in Fig. 1c, which range in length from 38 to 48 residues. C-terminal amidation is another characteristic of ArCRH that is a conserved characteristic of CRH-related peptides. Furthermore, other evolutionarily conserved features highlighted with asterisks in Fig. 1c include the following residues in ArCRH, with positions in parentheses: LSV (3-5), I (11), R (13), L (16), QAE (29-31), N (33) and L (36).

Cellular localization of ArCRHP transcripts in A. rubens using mRNA in situ hybridization

Here mRNA *in situ* hybridization was employed to analyse expression of ArCRHP in *A. rubens*, revealing a widespread pattern of expression including the central nervous system (Fig. 2), digestive system (Fig. 3) and body-wall associated structures (Fig. 4).

Central nervous system

The central nervous system of *A. rubens* comprises five radial nerve cords linked by a circumoral nerve ring situated in the central disk region. Both the radial nerve cord and circumoral nerve ring comprise two distinct regions: the ectoneural region and the hyponeural region, which contains the cell bodies of motoneurons [40]. Anti-sense probes revealed ArCRHP-expressing cells in both the ectoneural and hyponeural regions of the radial nerve cords (Fig. 2a-e) and the specificity of staining observed with anti-sense probes was confirmed by control experiments using sense probes, where no staining was observed (Fig. 2a inset). Examination of the distribution of ArCRHP-expressing cells in transverse sections of the radial nerve cord revealed that stained cells are distributed throughout the epithelial layer of the ectoneural region, whereas in the hyponeural region only a single stained cell was observed (Fig. 2a-c). Accordingly, examination of longitudinal sections of the radial nerve cord revealed stained cells along the length of the ectoneural epithelium but with only a single stained cell observed in the hyponeural region (Fig. 2d,e). Consistent with the pattern of ArCRHP expression in the radial nerve cords, stained cells were revealed in both the ectoneural and hyponeural regions of the circumoral nerve ring. However, the relative abundance of stained cells in the circumoral nerve ring was higher than in the radial

nerve cords, with densely packed clusters of stained cells in the ectoneural region and several stained cells in the hyponeural region being revealed in transverse sections (Fig. 2f-h).

Digestive system

Cells expressing ArCRHP were revealed in the cardiac stomach (Fig. 3a,b) and pyloric stomach (Fig. 3c,d) and in both regions of the stomach the stained cells are located within the mucosal layer but in close proximity to the basiepithelial nerve plexus layer (Fig. 3b,d). Stained cells were also revealed in the pyloric ducts that link the pyloric stomach with the paired pyloric caeca (digestive organs) located in each arm, with the ArCRHP-expressing cells located on the aboral side of the pyloric duct (Fig. 3e,f). Stained cells were also revealed in the pyloric caeca (Fig. 3g,h), located in the duct region of each pyloric caecum diverticulum.

Apical muscle

The apical muscle is located in a sagittal and aboral position along the coelomic lining of each arm in *A. rubens*. ArCRHP-expressing cells were revealed in the coelomic epithelium of the apical muscle, as shown in here in both transverse (Fig. 4a,b) and longitudinal (Fig. 4c,d) sections of arms.

Characterisation of a rabbit antiserum to ArCRH using ELISA

To test for the presence of antibodies to ArCRH in antiserum from a rabbit that had been immunised with a conjugate of thyroglobulin and an ArCRH antigen peptide (ArCRH-ag), serum from the second bleed was prepared at dilutions ranging from 1:500 and 1:128000 and incubated with a fixed amount of ArCRH-ag in a microtitre plate (1×10^{-10} moles/well). In parallel, pre-immune serum was tested in the same way and experiments without any added serum were also performed. No immunoreactivity was detected in wells containing pre-immune serum, but immunoreactivity was detected with the antiserum at dilutions ranging from 1:500 to 1: 32,000 (Supplemental Fig. 4a). To assess the sensitivity of the antiserum for detection of ArCRH-ag, the antiserum (diluted at 1:16000) was incubated with different amounts ArCRH-ag ranging from 1×10^{-9} moles to 1×10^{-16} moles. At this antiserum dilution, 1×10^{-9} - 1×10^{-11} moles of the antigen peptide could be detected in (Supplemental Fig. 4b). Collectively, these ELISA results demonstrated that antibodies to ArCRH were generated successfully. Furthermore, the finding that even at antiserum dilutions as low as 1:32,000 ArCRH-ag could be detected indicates that the antiserum contains a high titre of antibodies to the ArCRH. Accordingly, the ArCRH antiserum was used for immunohistochemical analysis of ArCRH expression in *A. rubens* (see below) at a dilution of 1:32,000.

Immunohistochemical localisation of ArCRH in A. rubens

Immunohistochemical analysis using the ArCRH antiserum revealed that ArCRH-immunoreactive cells and processes are widely distributed in *A. rubens*, including in the nervous system (Fig. 5), tube feet (Fig. 6), the digestive system (Fig. 7 and 8) and body-wall associated structures (Fig. 9).

Nervous system

Intense ArCRH-immunoreactivity was detected in the radial nerve cords and circumoral nerve ring of *A. rubens* (Fig. 5a,b). Importantly the specificity of the immunostaining observed with the ArCRH antiserum was confirmed by pre-absorption control experiments (Fig. 5b inset). Figure 5a provides an overview of the distribution of ArCRH in the nervous system in a horizontal section of a juvenile starfish, with immunostaining revealed in the circumoral nerve, the radial nerve cords and the marginal nerves, which run parallel to the outer row of tube feet on each side of the arms.

Analysis of immunostaining in transverse sections of the radial nerve cord revealed that the distribution of stained cells (Fig. 5b) is highly consistent with the distribution of ArCRHP transcripts revealed using mRNA *in situ* hybridisation (see Fig. 2). Thus, stained cells can be seen throughout much of the epithelial layer of the ectoneural region but are absent at the apex of the V-shaped nerve cord. Furthermore, use of immunohistochemistry enabled visualisation of ArCRH in the dense fibre network of the underlying neuropile of the ectoneural region (Fig. 5b,c). Also, the bipolar shape of the ectoneural ArCRH-immunoreactive cells can be seen in Figure 5c. In the hyponeural region only a single stained cell can be seen in the transverse section shown in Figure 5b and at higher magnification in Figure 5d, consistent with findings from use of mRNA *in situ* hybridisation for localisation of ArCRHP transcripts.

At the margins of the radial nerve cord, immunostaining in the ectoneural neuropile is continuous with immunostaining in the sub-epithelial nerve plexus of adjacent tube feet, whilst immunostained processes derived from the hyponeural region project around the margin of the peri-hemal canal (Fig. 5e). High magnification images of transverse sections of the marginal nerve cord reveal that immunostaining in the neuropile of the

marginal nerve is continuous with staining in the sub-epithelial nerve plexus of an adjacent tube foot. The pattern of immunostaining in the circumoral nerve ring (Fig. 5g) is consistent with that in radial nerve cord, with stained bipolar cells in the ectoneural epithelium and stained processes in the underlying neuropile. Immunostained fibres are evident in the hyponeural region (Fig. 5g), consistent with expression of ArCRHP transcripts in cells revealed by mRNA *in situ* hybridisation.

Tube feet

Immunostaining is present throughout the sub-epithelial nerve plexus of tube foot podia and extending into the basal nerve ring (Fig. 5f; Fig. 6a-c). No immunostained cell bodies were observed in tube feet, indicating that the immunostaining in sub-epithelial nerve plexus is associated with fibres derived from cells located in the adjacent ectoneural epithelium of the radial nerve cord. Immunostained fibres were also revealed in the muscle layer of tube foot podia (Fig. 5f; 6b). Immunostaining is also present in tube foot ampullae, and here it is located in fibres underlying the coelomic epithelial layer and in fibres in the muscle layer (Fig. 6d,e).

Digestive system

Immunostaining was revealed in the peristomial membrane (Fig. 7a), where it is localised in the basiepithelial nerve plexus located beneath the external epithelial layer and in a nerve plexus located beneath the coelomic epithelial lining (Fig. 7b). Accordingly, immunostained cells were also observed in close proximity to the immunostained plexi (Fig. 7b). A similar pattern of immunostaining to that observed in the peristomial membrane is seen in the esophagus (Fig. 7c). Immunostaining was also observed in the cardiac stomach, most notably in the highly folded lateral pouches proximal to intrinsic retractor strands (Fig. 7d-h) [41]. Furthermore, immunostaining was not evenly distributed throughout the folds of the cardiac stomach, with immunostaining most intense in the mucosal basiepithelial plexus and associated cells adjacent to intrinsic retractor strands and with immunostaining least intense in intervening sections of the stomach wall (Fig. 7d-f). Accordingly, in small juvenile starfish where it is possible to view an entire horizontal section of the cardiac stomach, immunostaining can be seen to be concentrated in regions of the basiepithelial nerve plexus adjacent to sites of attachment of the extrinsic retractor strands (Fig. 7g,h).

In the pyloric stomach, immunostaining was widely distributed throughout the basiepithelial nerve plexus, as seen in both transverse (Fig. 7d) and horizontal (Fig. 8a) sections of the central disk region. At high magnification it can be observed that immunostained fibres in the basiepithelial nerve plexus are derived from immunostained cells located at the boundary between the nerve plexus and the mucosa (Fig. 8b). Immunostaining associated with the basiepithelial nerve plexus also extends into the pyloric ducts, which link the pyloric stomach to the paired pyloric caeca located in each arm (Fig. 8a,c). In the pyloric caeca, the pattern of immunostaining is inhomogeneous and this can be observed in both horizontal (Fig. 8a,d) and transverse (Fig. 8f,i) sections of pyloric caeca. Immunostaining is most prominent at the apex of the oral side of the pyloric duct regions of the pyloric caeca, whereas in diverticulae immunostaining is less prominent (Fig. 8a; arrow and arrowhead). Furthermore, high magnification images of the ducts reveal that immunostaining is localised in both the basiepithelial nerve plexus of the mucosal layer and in the nerve plexus located beneath the coelomic epithelial lining (Fig. 8h; arrow and arrowhead). Lastly, no staining was observed in the rectal caeca (Fig. 8j) but immunostaining was observed in the basiepithelial nerve plexus of the rectum (Fig. 8j,k) and in both the basiepithelial nerve plexus and sub-coelomic nerve plexus of the intestine (Fig. 8j,l).

Body-wall associated structures

In the body wall, immunostained processes are present proximal to the circular muscle layer and in the coelomic basiepithelial nerve plexus (Fig. 9a,b). Immunostained cells are present in the coelomic epithelial layer of the apical muscle (Fig. 9b) and immunostained processes derived from these cells ramify amongst the longitudinally orientated muscle fibres of the apical muscle (Fig. 9b). The immunostained nerve plexi associated with the longitudinally and circularly orientated muscle layers of the body wall also extend into the walls of papulae, finger-shaped appendages that enable gas exchange between the coelomic fluid and the external seawater (Fig. 9a,c). Immunostaining is also present in the sub-epithelial nerve plexus of the external body wall epithelium (Fig. 9d).

Discussion

In this paper we report the first analysis of the molecular structure and expression of a CRH-type neuropeptide in an echinoderm – the starfish *Asterias rubens*. Previous studies have reported the sequencing of a cDNA encoding the precursor of an *A. rubens* CRH-type neuropeptide (ArCRH) [36, 35]. Here mass spectrometric analysis of extracts of radial nerve cords from *A. rubens* enabled determination of the mature structure of ArCRH, revealing that it is a 40-residue peptide with N-terminal pyroglutamylation and C-terminal amidation. The frog skin peptide sauvagine, which was the first CRH-type peptide to be sequenced, also has an N-terminal pyroglutamate[7]. However, this is not a conserved feature of CRH-type peptides; for example, human CRH and urocortins do not have an N-terminal pyroglutamate (Fig 1c). In contrast, C-terminal amidation is a conserved feature of CRH-type peptides (Fig. 1c). Furthermore, comparison of the sequence of ArCRH with CRH and related neuropeptides in other taxa revealed other conserved structural characteristics, as highlighted with asterisks in Fig. 1c. It is noteworthy that the conserved residues are predominantly located within the N-terminal and C-terminal regions of the peptide, with the central region of the peptide (residues 17-28) exhibiting less sequence conservation with other CRH-type peptides. This is interesting because the N- and C-terminal regions of mammalian CRH-type peptides are involved in receptor binding/activation [42]. Therefore, it is likely that these regions are also important for the bioactivity of ArCRH.

Cloning and sequencing of a cDNA encoding the ArCRH precursor (ArCRH) has previously enabled generation of labelled RNA probes for ArCRHP transcripts, which have been employed for cellular localisation of ArCRHP expression in *A. rubens* larvae using mRNA *in situ* hybridisation techniques [36]. No expression of ArCRHP was observed during early larval development in the two-armed bipinnariae, but in brachiolaria larvae ArCRHP-expressing cells were observed in the brachia and in tissue adjacent to the adhesive disk [36]. The adhesive disk mediates larval attachment to the substratum prior to metamorphosis of the bilaterally symmetrical larval stage into a pentaradially symmetrical juvenile [43, 44]. Therefore, we speculated that ArCRH may be involved in regulation of physiological processes associated with larval attachment [36].

Here mRNA *in situ* hybridisation was employed to investigate ArCRHP expression for the first time in post-metamorphic juvenile and adult starfish. Furthermore, determination of the mature structure of ArCRH provided a basis for generation of a specific antibodies to the C-terminal region of this peptide. Characterisation of an ArCRH rabbit antiserum using ELISA revealed a high titre of antibodies to the C-terminal region of ArCRH, enabling use of a highly diluted antiserum (1:32,000) for immunohistochemical localisation of ArCRH. Analysis of the distribution of ArCRHP transcripts and ArCRH peptide in *A. rubens* using mRNA *in situ* hybridisation and immunohistochemistry, respectively, revealed mutually consistent patterns of stained cells. Furthermore, immunohistochemistry enabled visualisation of the stained axonal processes of ArCRH-expressing neurons in *A. rubens*. Informed by the pattens of ArCRHP/ArCRH expression in the *A. rubens*, we present below a functional interpretation and discussion of our findings.

In the central nervous system of *A. rubens*, which comprises the circumoral nerve ring and five radial nerve cords, ArCRH-expressing cells were revealed in both the ectoneural and hyponeural regions. The ectoneural region receives and integrates input from sensory cells located throughout the external epithelium of the body surface and accordingly it has an extensive neuropile layer [40]. ArCRH-expressing cells were revealed in the epithelium of the ectoneural region and in the underlying neuropile a dense population of ArCRH-immunoreactive fibres was revealed. These findings are generally consistent with previous analyses of the expression of other neuropeptides, although specific differences in the patterns of ectoneural neuropeptide expression in *A. rubens* are observed. The hyponeural region of the CNS in starfish and other echinoderms contains segmental clusters (ganglia) of motoneuronal cell bodies and the activity of these neurons is driven by input from ectoneural neurons [40, 45]. In this context, it is noteworthy that typically only a single ArCRH-immunoreactive hyponeural cell body was observed in transverse sections of the radial nerve cord in *A. rubens*. This contrasts with other neuropeptides such as pedal peptide/orcokinin-type, gonadotropin-releasing hormone-type, calcitonin-type and somatostatin-type peptides, where several cell bodies expressing these neuropeptides were observed in transverse sections of the radial nerve cord in *A. rubens* [38, 31, 32, 46, 34]. However, in sections of the circumoral nerve ring of *A. rubens*, several ArCRH-immunoreactive cell bodies were typically revealed in the hyponeural region, indicating regional differences in hyponeural ArCRH expression in the *A. rubens* CNS. The functional significance of differences in patterns of hyponeural neuropeptide expression in *A. rubens* is not known. However, analysis of peripheral expression of neuropeptides in the axons of hyponeural motoneurons may be informative. For example, one interesting feature of ArCRH expression in *A. rubens* is the presence of ArCRH-immunoreactive fibres in the muscle layer of the ampulla and podium of tube feet. This is

noteworthy because hitherto we have not observed expression of other neuropeptides in nerve fibres located within the muscle layer of tube feet. Conversely, motor fibres innervating interossicular muscles of the body wall in *A. rubens* are immunoreactive with antibodies to other neuropeptides (e.g. pedal peptide/orcokinin-type and calcitonin-type;[38, 32, 46], but these nerve fibres were not observed to be immunoreactive with ArCRH antibodies in this study. Thus, comparative analysis of neuropeptide expression provides a basis for identification of different populations of hyponeural neurons, and our findings reported here indicate that ArCRH is expressed in a sub-population of hyponeural motoneurons that directly innervate the muscle layer in the podium and ampulla of tube feet in *A. rubens*. Furthermore, ArCRH-immunoreactivity is also present in other compartments of the nervous system associated with tube feet, including nerve fibres located within the coelomic lining of the ampulla and nerve fibres located in the sub-epithelial nerve plexus and basal nerve ring of the podium. Therefore, ArCRH may participate in a variety of neural mechanisms associated with regulation of tube foot activity, with potential relevance to behaviours that involve tube feet (e.g. locomotion and feeding).

Gas exchange in starfish is mediated by protractible organs called papulae, which penetrate through the body wall skeleton and provide a thin-walled surface for gas exchange between external seawater and coelomic fluid that bathes visceral organs [47]. ArCRH-immunoreactivity was revealed in the innervation of papulae, which is derived from the axons of hyponeural motoneurons associated with the circular muscle layer of the body wall and the apical nervous system associated with the longitudinal muscle layer of the body wall. Consistent with the latter, ArCRHP/ArCRH expressing cells were revealed in aboral coelomic lining of the body wall and ArCRH-immunoreactive nerve fibres were revealed within the apical muscle, a thickened strand of longitudinally orientated muscle that facilitates arm flexion. Therefore, ArCRH may participate in neural mechanisms associated with regulation of papula protraction/retraction and control of the circularly and longitudinally orientated muscle layers of the body wall in *A. rubens*.

A widespread pattern of ArCRH expression was observed in the digestive system of *A. rubens*, including the peristomial membrane that surrounds the mouth, esophagus, cardiac stomach, pyloric stomach, pyloric ducts, pyloric caeca, intestine and rectum. ArCRH-immunoreactive cells were revealed in the gut mucosal layer, with immunostained processes contributing to staining in the basiepithelial nerve plexus. Based on these characteristics, the ArCRH-immunoreactive cells in the gut mucosa can be classified as enteric neurons with axonal processes and/or endocrine cells with neuropods [48], but detailed ultrastructural analysis will be required for a more precise identification of cell types expressing ArCRH in the starfish digestive system. ArCRH-immunoreactivity was also revealed in the visceral nerve plexus, which is located beneath the coelomic epithelium of the gut. The extensive expression of ArCRH throughout much of the digestive system in *A. rubens* is indicative of a general role in regulation of gut function. Noteworthy in this respect is the variation in the intensity or density of immunostaining in the basiepithelial nerve plexus within regions of the gut. For example, in the cardiac stomach immunostaining is stronger in regions adjacent to the intrinsic retractor strands and in the pyloric caeca immunostaining is stronger in the pyloric duct region than in the diverticulae. Variation in the intensity/density of immunostaining within regions of the gut has been also observed for other neuropeptides in *A. rubens*; for example, the calcitonin-type neuropeptide ArCT [32]. However, its functional significance remains to be elucidated. The higher concentration of ArCRH-immunoreactivity in the pyloric duct region of the pyloric caeca could be informative in this respect because this region of the gut is involved in ciliary-mediated transport of food material [49]. Therefore, ArCRH may be involved in neural regulation of these processes in the digestive system of *A. rubens*.

The extensive expression of ArCRH in *A. rubens* is clearly indicative of roles in regulation of a variety of physiological processes, as discussed above. Therefore, it is of interest to consider more broadly what is known about the physiological roles of CRH-related peptides in other taxa. In mammals CRH is, of course, known for its role in mediating physiological adaptations to stressors, stimulating pituitary secretion of ACTH that leads to adrenal release of cortisol. However, CRH and its paralogue UCN also have behavioural effects associated with adaptation to stressors and novel environments, including increased arousal, decreased food intake, reduced sexual and reproductive activity and increased grooming. Thus, it is proposed that CRH/UCN acting via the CRF1 receptor in the CNS integrates physiological and behavioural responses to stressors [50]. Interestingly, it has been proposed that these actions of CRH/UCN may be reflective of a highly specialised role in mammals, with the actions of UCN2 and UNC3 perhaps being more representative of the neuropeptide family as a whole. In this context, it is noteworthy that UCN2/UCN3 acting via CRF2 have anxiolytic effects and roles in energy homeostasis, with UCN2 increasing tissue sensitivity to insulin and UCN3 increasing pancreatic secretion of insulin [50].

Furthermore, investigation of the expression and actions of a CRH-type peptide in the invertebrate chordate *C. intestinalis* has revealed evidence of roles in inhibitory regulation of feeding behaviour [51].

Turning now to protostome invertebrates, here our knowledge of CRH-type neuropeptide function draws largely from investigation of the physiological roles of the CRH-like diuretic hormone DH44 in *Drosophila melanogaster*. This has revealed that, in addition to its diuretic action [52-54], DH44 has roles in regulation of a variety of processes, including circadian locomotor activity [55-57], feeding [58, 53, 59, 54] and sperm retention/storage in post-copulatory females [60]. With respect to the latter function, it is noteworthy that egg-laying hormone (ELH) in *Aplysia californica* and in other gastropod molluscs has been identified as a DH44-like peptide [61-63, 18, 64]. Therefore, DH44/ELH-type neuropeptides may have evolutionarily conserved roles as regulators of reproductive processes in protostomes. Further studies on a wider range of taxa are now needed to gain broader insights into the physiological roles of DH44-type neuropeptides in protostomes.

In conclusion, our detailed analysis of the expression pattern of the CRH-type neuropeptide ArCRH in an echinoderm, the starfish *A. rubens*, provides an anatomical basis for experimental investigation of its physiological roles and comparison with the findings from chordates and protostome invertebrates discussed above. It will also be of interest to investigate the expression and physiological roles of CRH-type neuropeptides in other echinoderms. Thus far, precursors of ArCRH-like neuropeptides have not been identified in echinoids (e.g. sea urchins), holothurians (sea cucumbers) or crinoids (e.g. featherstars). However, four precursors of ArCRH-like neuropeptides have been identified in an ophiuroid species, the brittle star *Ophionotus victoriae* [65]. Investigation of the expression of CRH-type precursors in *O. victoriae* and/or other brittle stars would enable comparison with findings reported here for ArCRH in the starfish *A. rubens* and exploration of the physiological significance of gene duplication giving rise to multiple CRH-type neuropeptide precursors in these animals.

Acknowledgments
We are grateful to Phil Edwards for his help with obtaining starfish and to Paul Fletcher and Ian Sanders for maintaining our seawater aquarium.
Statement of Ethics
Approval by the local institution/ethics committee was not required for this work because experimental work on starfish is not subject to regulation.
Conflict of Interest Statement
The authors declare that the research was conducted in the absence of any commercial or financial relationships that could be construed as a potential conflict of interest.
Funding Sources
WC was supported by a China Scholarship Council studentship; MRE and ME were supported by a grant from the BBSRC (BB/M001644/1); AJ and CZ were supported by a grant from the BBSRC (BB/M001032/1).
Author Contributions
WC, ME, and MRE carried out the analysis of the expression of ArCRHP and ArCRH using mRNA *in situ* hybridization and immunohistochemistry. WC carried out the sequence and phylogenetic analysis of ArCRH and examination of the *in vitro* pharmacological effects of ArCRH. CZ and AJ carried out the structural characterization of ArCRH using mass spectrometry. The paper was written by WC and MRE, with contributions from other authors. The study was conceived and designed by MRE. All authors gave final approval for publication.

References

1. Harris G, DeGroot J. Hypothalamic control of the secretion of adrenocorticotropic hormone. FEDERATION PROCEEDINGS: FEDERATION AMER SOC EXP BIOL 9650 ROCKVILLE PIKE, BETHESDA, MD 20814-3998; 1950. p. 57-57.
2. Guillemin R, Rosenberg B. Humoral hypothalamic control of anterior pituitary: a study with combined tissue cultures. Endocrinology. 1955 Nov;57(5):599-607.
3. Saffran M, Schally AV. In vitro bioassay of corticotropin: modification and statistical treatment. Endocrinology. 1955 May;56(5):523-32.
4. Vale W, Spiess J, Rivier C, Rivier J. Characterization of a 41-residue ovine hypothalamic peptide that stimulates secretion of corticotropin and β-endorphin. Science. 1981:1394-97.
5. Furutani Y, Morimoto Y, Shibahara S, Noda M, Takahashi H, Hirose T, et al. Cloning and sequence analysis of cDNA for ovine corticotropin-releasing factor precursor. Nature. 1983 Feb 10;301(5900):537-40.
6. Shibahara S, Morimoto Y, Furutani Y, Notake M, Takahashi H, Shimizu S, et al. Isolation and sequence analysis of the human corticotropin-releasing factor precursor gene. EMBO J. 1983;2(5):775-9.
7. Montecucchi PC, Henschen A, Erspamer V. Structure of sauvagine, a vasoactive peptide from the skin of a frog. Hoppe Seylers Z Physiol Chem. 1979;360:1170.
8. Ichikawa T, McMaster D, Lederis K, Kobayashi H. Isolation and amino acid sequence of urotensin I, a vasoactive and ACTH-releasing neuropeptide, from the carp (Cyprinus carpio) urophysis. Peptides. 1982 Sep-Oct;3(5):859-67.
9. Lederis K, Letter A, McMaster D, Moore G, Schlesinger D. Complete amino acid sequence of urotensin I, a hypotensive and corticotropin-releasing neuropeptide from Catostomus. Science. 1982 Oct 8;218(4568):162-5.
10. Hsu SY, Hsueh AJ. Human stresscopin and stresscopin-related peptide are selective ligands for the type 2 corticotropin-releasing hormone receptor. Nat Med. 2001 May;7(5):605-11.
11. Lewis K, Li C, Perrin MH, Blount A, Kunitake K, Donaldson C, et al. Identification of urocortin III, an additional member of the corticotropin-releasing factor (CRF) family with high affinity for the CRF2 receptor. Proc Natl Acad Sci U S A. 2001 Jun 19;98(13):7570-5.
12. Reyes T, Lewis K, Perrin M, Kunitake K, Vaughan J, Arias C, et al. Urocortin II: a member of the corticotropin-releasing factor (CRF) neuropeptide family that is selectively bound by type 2 CRF receptors. Proceedings of the National Academy of Sciences. 2001;98(5):2843-48.
13. Chen R, Lewis KA, Perrin MH, Vale WW. Expression cloning of a human corticotropin-releasing-factor receptor. Proc Natl Acad Sci U S A. 1993 Oct 1;90(19):8967-71.
14. Perrin M, Donaldson C, Chen R, Blount A, Berggren T, Bilezikjian L, et al. Identification of a second corticotropin-releasing factor receptor gene and characterization of a cDNA expressed in heart. Proc Natl Acad Sci U S A. 1995 Mar 28;92(7):2969-73.
15. Lovejoy DA, Chang BS, Lovejoy NR, del Castillo J. Molecular evolution of GPCRs: CRH/CRH receptors. J Mol Endocrinol. 2014 Jun;52(3):T43-60.
16. Cardoso JC, Bergqvist CA, Félix RC, Larhammar D. Corticotropin-releasing hormone family evolution: five ancestral genes remain in some lineages. Journal of molecular endocrinology. 2016;57(1):73-86.
17. Lovejoy DA, Barsyte-Lovejoy D. Characterization of a corticotropin-releasing factor (CRF)/diuretic hormone-like peptide from tunicates: insight into the origins of the vertebrate CRF family. General and comparative endocrinology. 2010;165(2):330-36.
18. Mirabeau O, Joly JS. Molecular evolution of peptidergic signaling systems in bilaterians. Proc Natl Acad Sci U S A. 2013 May 28;110(22):E2028-37.
19. Kataoka H, Troetschler RG, Li JP, Kramer SJ, Carney RL, Schooley DA. Isolation and identification of a diuretic hormone from the tobacco hornworm, Manduca sexta. Proc Natl Acad Sci U S A. 1989 Apr;86(8):2976-80.
20. Reagan JD. Expression cloning of an insect diuretic hormone receptor. A member of the calcitonin/secretin receptor family. J Biol Chem. 1994 Jan 7;269(1):9-12.
21. Johnson EC, Bohn LM, Taghert PH. Drosophila CG8422 encodes a functional diuretic hormone receptor. J Exp Biol. 2004 Feb;207(Pt 5):743-8.
22. Hector CE, Bretz CA, Zhao Y, Johnson EC. Functional differences between two CRF-related diuretic hormone receptors in Drosophila. Journal of Experimental Biology. 2009;212(19):3142-47.
23. De Oliveira AL, Calcino A, Wanninger A. Extensive conservation of the proneuropeptide and peptide prohormone complement in mollusks. Sci Rep. 2019 Mar 19;9(1):4846.

24. Elphick MR, Mirabeau O, Larhammar D. Evolution of neuropeptide signalling systems. J Exp Biol. 2018 Feb 9;221(Pt 3).
25. Semmens DC, Elphick MR. The evolution of neuropeptide signalling: insights from echinoderms. Brief Funct Genomics. 2017 Sep 1;16(5):288-98.
26. Semmens DC, Beets I, Rowe ML, Blowes LM, Oliveri P, Elphick MR. Discovery of sea urchin NGFFFamide receptor unites a bilaterian neuropeptide family. Open Biol. 2015 Apr;5(4):150030.
27. Tinoco AB, Semmens DC, Patching EC, Gunner EF, Egertová M, Elphick MR. Characterization of NGFFYamide signaling in starfish reveals roles in regulation of feeding behavior and locomotory systems. Frontiers in Endocrinology. 2018;9:507.
28. Tian S, Zandawala M, Beets I, Baytemur E, Slade SE, Scrivens JH, et al. Urbilaterian origin of paralogous GnRH and corazonin neuropeptide signalling pathways. Sci Rep. 2016 Jun 28;6:28788.
29. Zandawala M, Tian S, Elphick MR. The evolution and nomenclature of GnRH-type and corazonin-type neuropeptide signaling systems. Gen Comp Endocrinol. 2018 Aug 1;264:64-77.
30. Yanez-Guerra LA, Zhong X, Moghul I, Butts T, Zampronio CG, Jones AM, et al. Echinoderms provide missing link in the evolution of PrRP/sNPF-type neuropeptide signalling. Elife. 2020 Jun 24;9.
31. Tian S, Egertová M, Elphick MR. Functional characterization of paralogous gonadotropin-releasing hormone-type and corazonin-type neuropeptides in an echinoderm. Frontiers in endocrinology. 2017;8:259.
32. Cai W, Kim C-H, Go H-J, Egertová M, Zampronio CG, Jones AM, et al. Biochemical, anatomical, and pharmacological characterization of calcitonin-type neuropeptides in starfish: discovery of an ancient role as muscle relaxants. Frontiers in neuroscience. 2018;12:382.
33. Odekunle EA, Semmens DC, Martynyuk N, Tinoco AB, Garewal AK, Patel RR, et al. Ancient role of vasopressin/oxytocin-type neuropeptides as regulators of feeding revealed in an echinoderm. BMC biology. 2019;17(1):60.
34. Zhang Y, Yanez Guerra LA, Egertova M, Zampronio CG, Jones AM, Elphick MR. Molecular and functional characterization of somatostatin-type signalling in a deuterostome invertebrate. Open Biol. 2020 Sep;10(9):200172.
35. Semmens DC, Mirabeau O, Moghul I, Pancholi MR, Wurm Y, Elphick MR. Transcriptomic identification of starfish neuropeptide precursors yields new insights into neuropeptide evolution. Open biology. 2016;6(2):150224.
36. Mayorova TD, Tian S, Cai W, Semmens DC, Odekunle EA, Zandawala M, et al. Localization of Neuropeptide Gene Expression in Larvae of an Echinoderm, the Starfish Asterias rubens. Front Neurosci. 2016;10:553.
37. Lin M, Mita M, Egertova M, Zampronio CG, Jones AM, Elphick MR. Cellular localization of relaxin-like gonad-stimulating peptide expression in Asterias rubens: New insights into neurohormonal control of spawning in starfish. J Comp Neurol. 2017 May 01;525(7):1599-617.
38. Lin M, Egertova M, Zampronio CG, Jones AM, Elphick MR. Pedal peptide/orcokinin-type neuropeptide signaling in a deuterostome: The anatomy and pharmacology of starfish myorelaxant peptide in Asterias rubens. J Comp Neurol. 2017 Dec 15;525(18):3890-917.
39. Skowsky WR, Fisher DA. The use of thyroglobulin to induce antigenicity to small molecules. The Journal of laboratory and clinical medicine. 1972 Jul;80(1):134-44.
40. Pentreath VW, Cobb JL. Neurobiology of echinodermata. Biol Rev Camb Philos Soc. 1972 Aug;47(3):363-92.
41. Anderson JM. Studies on the cardiac stomach of the starfish, Asterias forbesi. The Biological Bulletin. 1954;107(2):157-73.
42. Deussing JM, Chen A. The Corticotropin-Releasing Factor Family: Physiology of the Stress Response. Physiol Rev. 2018 Oct 1;98(4):2225-86.
43. Haesaerts D, Jangoux M, Flammang P. The attachment complex of brachiolaria larvae of the sea star Asterias rubens (Echinodermata): an ultrastructural and immunocytochemical study. Zoomorphology. 2005;124(2):67-78.
44. Murabe N, Hatoyama H, Komatsu M, Kaneko H, Nakajima Y. Adhesive papillae on the brachiolar arms of brachiolaria larvae in two starfishes, Asterina pectinifera and Asterias amurensis, are sensors for metamorphic inducing factor (s). Development, growth & differentiation. 2007;49(8):647-56.
45. Cobb JL. The neurobiology of the ectoneural/hyponeural synaptic connection in an echinoderm. The Biological Bulletin. 1985;168(3):432-46.

46. Lin M, Egertová M, Zampronio CG, Jones AM, Elphick MR. Functional characterization of a second pedal peptide/orcokinin‐type neuropeptide signaling system in the starfish Asterias rubens. Journal of Comparative Neurology. 2018;526(5):858-76.
47. Cobb J. An ultrastructural study of the dermal papulae of the starfish, Asterias rubens, with special reference to innervation of the muscles. Cell and tissue research. 1978;187(3):515-23.
48. Garcia-Arraras JE, Lefebre-Rivera M, Qi-Huang S. Enteroendocrine cells in the Echinodermata. Cell Tissue Res. 2019 Sep;377(3):459-67.
49. Jangoux M. 2. ETUDE STRUCTURELLE ET FONCTIONNELLE DU TUBE DIGESTIF D'ASTERIAS RUBENS L.(ECHINODERMATA: ASTEROIDEA). Aust Mus Mem. 1982;16:17-38.
50. Lovejoy DA, de Lannoy L. Evolution and phylogeny of the corticotropin-releasing factor (CRF) family of peptides: expansion and specialization in the vertebrates. Journal of chemical neuroanatomy. 2013;54:50-56.
51. Andrea L, Hsieh AH-R, Hsieh AH-M, De Almeida R, Lovejoy SR, Lovejoy DA. Expression and actions of corticotropin-releasing factor/diuretic hormone-like peptide (CDLP) and teneurin C-terminal associated peptide (TCAP) in the vase tunicate, Ciona intestinalis: antagonism of the feeding response. General and comparative endocrinology. 2017;246:105-15.
52. Cabrero P, Radford JC, Broderick KE, Costes L, Veenstra JA, Spana EP, et al. The Dh gene of Drosophila melanogaster encodes a diuretic peptide that acts through cyclic AMP. Journal of Experimental Biology. 2002;205(24):3799-807.
53. Cannell E, Dornan AJ, Halberg KA, Terhzaz S, Dow JAT, Davies SA. The corticotropin-releasing factor-like diuretic hormone 44 (DH44) and kinin neuropeptides modulate desiccation and starvation tolerance in Drosophila melanogaster. Peptides. 2016 Jun;80:96-107.
54. Zandawala M, Marley R, Davies SA, Nässel DR. Characterization of a set of abdominal neuroendocrine cells that regulate stress physiology using colocalized diuretic peptides in Drosophila. Cellular and Molecular Life Sciences. 2018;75(6):1099-115.
55. Cavanaugh DJ, Geratowski JD, Wooltorton JR, Spaethling JM, Hector CE, Zheng X, et al. Identification of a circadian output circuit for rest:activity rhythms in Drosophila. Cell. 2014 Apr 24;157(3):689-701.
56. Cavey M, Collins B, Bertet C, Blau J. Circadian rhythms in neuronal activity propagate through output circuits. Nature neuroscience. 2016;19(4):587.
57. King AN, Barber AF, Smith AE, Dreyer AP, Sitaraman D, Nitabach MN, et al. A Peptidergic Circuit Links the Circadian Clock to Locomotor Activity. Curr Biol. 2017 Jul 10;27(13):1915-27 e5.
58. Dus M, Lai JS, Gunapala KM, Min S, Tayler TD, Hergarden AC, et al. Nutrient Sensor in the Brain Directs the Action of the Brain-Gut Axis in Drosophila. Neuron. 2015 Jul 1;87(1):139-51.
59. Yang Z, Huang R, Fu X, Wang G, Qi W, Mao D, et al. A post-ingestive amino acid sensor promotes food consumption in Drosophila. Cell Res. 2018 Oct;28(10):1013-25.
60. Lee K-M, Daubnerová I, Isaac RE, Zhang C, Choi S, Chung J, et al. A neuronal pathway that controls sperm ejection and storage in female Drosophila. Current Biology. 2015;25(6):790-97.
61. Chiu AY, Hunkapiller MW, Heller E, Stuart DK, Hood LE, Strumwasser F. Purification and primary structure of the neuropeptide egg-laying hormone of Aplysia californica. Proc Natl Acad Sci U S A. 1979 Dec;76(12):6656-60.
62. Scheller RH, Jackson JF, McAllister LB, Schwartz JH, Kandel ER, Axel R. A family of genes that codes for ELH, a neuropeptide eliciting a stereotyped pattern of behavior in Aplysia. Cell. 1982;28(4):707-19.
63. Bernheim SM, Mayeri E. Complex behavior induced by egg-laying hormone in Aplysia. J Comp Physiol A. 1995 Jan;176(1):131-6.
64. Stewart MJ, Favrel P, Rotgans BA, Wang T, Zhao M, Sohail M, et al. Neuropeptides encoded by the genomes of the Akoya pearl oyster Pinctata fucata and Pacific oyster Crassostrea gigas: a bioinformatic and peptidomic survey. BMC genomics. 2014;15(1):1-16.
65. Zandawala M, Moghul I, Yanez Guerra LA, Delroisse J, Abylkassimova N, Hugall AF, et al. Discovery of novel representatives of bilaterian neuropeptide families and reconstruction of neuropeptide precursor evolution in ophiuroid echinoderms. Open Biol. 2017 Sep;7(9).

Figure legends

Fig. 1. Determination of the structure of the *A. rubens* CRH-type neuropeptide ArCRH and comparison of its sequence with CRH-related peptides in other taxa. (a). Amino acid sequence of the ArCRH precursor (GenBank accession number: KT601710.1); the predicted signal peptide is shown in blue, predicted dibasic/tribasic cleavage sites are shown in green and the predicted CRH-type peptide is shown in red, with its C-terminal glycine (G) residue that is a putative substrate for amidation shown in orange. **(b)**. The mature structure of ArCRH as determined by mass spectrometric analysis of *A. rubens* radial nerve cord extracts, with post-translational conversion of an N-terminal glutamine to pyroglutamate shown as pQ and conversion of a C-terminal glycine residue to an amide (a) shown in lowercase. Fragments of the ArCRH peptide for which structures were determined by mass spectrometry are indicated by the lines underneath the peptide sequence, with (brown) or without (purple) trypsin treatment of nerve cord extracts. The molecular mass divided by the charge state (m/z) of the peptide ions is shown for each fragment, with the charge state in parentheses. The mass spectrometric data for these peptide fragments are shown in Supplemental Fig. 3 **(c).** Alignment of ArCRH with CRH-related peptides in other taxa. Conserved residues highlighted in black or grey, with black signifying a higher level of sequence conservation than grey. Several of the conserved residues and the C-terminal amide group in ArCRH are highlighted with asterisks above the alignment. Underlining of the N-terminal glutamine (Q) in *A. rubens* CRH and *P. sauvagii* sauvagine signifies that this residue has been shown to be post-translationally converted to a pyroglutamate in the mature peptides. An N-terminal Q in two of the CRH-type peptides in the brittle star *Ophionotus victoriae* is likewise a potential substrate for pyroglutamylation, but this has not been proven experimentally so the Q is not underlined. The species/name for each peptide is highlighted with one of the following phylum-specific colours: yellow (Echinodermata), purple (Hemichordata), light blue (Chordata), Olive (Arthropoda). Species name abbreviations are: A.rub, *Asterias rubens*; O.vic, *Ophionotus victoriae*; S.kow, *Saccoglossus kowalevskii*; B.flo, *Branchiostoma floridae*; C.int, *Ciona intestinalis*; Psau, *Phyllomedusa sauvagii*; H.sap, *Homo sapiens*; D.mel, *Drosophila melanogaster*. The accession numbers for the sequences included in this alignment are in Supplemental table. 1.

Fig. 2. Localization of ArCRHP mRNA in the radial nerve cords and circumoral nerve ring of *Asterias rubens* using *in situ* hybridization. (a) Transverse section of a radial nerve cord that was incubated with antisense probes showing stained cells in both the ectoneural (arrowheads) and hyponeural (arrow) regions. In the ectoneural region, stained cells are distributed throughout the sub-cuticular epithelium, whereas only one stained cell can be seen in the hyponeural region. Higher magnification images of the boxed regions are shown in panels (b) and (c). The inset in (a) shows an absence of stained cells in a transverse section of a radial nerve cord incubated with sense probes, demonstrating the specificity of staining observed with antisense probes. (b) High magnification image of the apex of the V-shaped radial nerve cord showing that this region is largely devoid of stained cells; distal to the apex a single stained cell (arrowhead) can be seen in the ectoneural epithelium. (c) High magnification image of the lateral region of the radial nerve cord showing stained cells in both the ectoneural region (arrowheads) and the hyponeural region (arrow). (d) Longitudinal parasagittal section of a radial nerve cord showing that stained cells are distributed along its length in the ectoneural region (arrowheads). In the hyponeural region, a single stained cell can be seen (arrow). A higher magnification image of the boxed region is shown in (e). (e) Stained cells in the ectoneural epithelium (arrowheads) and hyponeural region (arrow) of the radial nerve cord. (f) Transverse section of the central disk region showing stained cells in both the ectoneural (arrowheads) and hyponeural (arrows) regions of the circumoral nerve ring. High magnification images of the boxed regions are displayed in panels (g) and (h). (g) Stained cells located in the ectoneural region of the circumoral nerve ring (arrowheads) close to its junction with the peristomial membrane, which also contains stained cells. (h) Stained cells in the ectoneural epithelium (arrowheads) and hyponeural region (arrows) of the circumoral nerve ring. Abbreviations: CONR, circumoral nerve ring; Ec, ectoneural region of radial nerve cord; Hy, hyponeural region of radial nerve cord; PM, peristomial membrane; RHS, radial hemal strand; RNC radial nerve cord; TF, tube foot; THS, transverse hemal strand. Scale bar: 100 µm in a, d and f; 50 µm in (a) inset; 25 µm in b, c, e, g and h.

Fig. 3. Localization of ArCRHP mRNA in the digestive system of *Asterias rubens* using *in situ* hybridization. (a) Stained cells in the cardiac stomach proximal to intrinsic retractor strands. The boxed region is shown at higher magnification in panel (b), where stained cells (arrows) are located proximal to the basiepithelial nerve plexus layer. (c) Transverse section through the central disk region showing stained cells in both the cardiac stomach and pyloric stomach. The boxed region in (c) is shown at a higher magnification in panel (d), where the stained cells (arrows) are located proximal to the basiepithelial nerve plexus layer in the pyloric stomach. (e,f) Transverse

section of a pyloric duct showing stained cells located on the oral side. The boxed region in (e) is shown at higher magnification in panel (f), where stained cells (arrows) can be seen to be located close to the basiepithelial nerve plexus layer. (g,h) Transverse section of an arm showing stained cells in the duct region of a pyloric caecum diverticulum. The boxed region in (g) is shown at higher magnification in panel (h), where the stained cells (arrows) are located in the duct region of a pyloric caecum diverticulum. Abbreviations: BNP, basi-epithelial nerve plexus layer; CE, coelomic epithelium; CS, cardiac stomach; CT, collagenous tissue layer; IRS, intrinsic retractor strand; Lu, lumen; PM, peristomial membrane; PS, pyloric stomach; VML, visceral muscle layer. Scale bar: 200 µm in a and g; 100 µm in c and e; 50 µm in b and h; 25 µm in d and f.

Fig. 4. Localization of ArCRHP mRNA in the apical muscle of *Asterias rubens* using *in situ* hybridisation. (a) Stained cells in a transverse section of an apical muscle; the boxed region is shown at higher magnification in panel (b), where stained cells (arrows) are located in the coelomic epithelial lining of the apical muscle. (c) Sagittal section of an arm showing the apical muscle and pyloric caecum. The boxed region is shown at higher magnification in panel (d), showing a stained cell (arrow) in the coelomic epithelial lining of the apical muscle. Abbreviations: AM, Apical Muscle; PC, Pyloric caecum. Scale bar: 100 µm in c, 50 µm in a, 12.5 µm in b and d.

Fig. 5. Immunohistochemical localization of ArCRH in the radial nerve cords, circumoral nerve ring and marginal nerve of *Asterias rubens*. (a) Horizontal section of a juvenile specimen showing the presence of immunostaining in the circumoral nerve ring, radial nerve cords and marginal nerves. (b) Immunostained transverse section of the V-shaped radial nerve cord showing the presence of ArCRH-immunoreactivity in both the ectoneural and hyponeural regions. In the ectoneural epithelial layer the stained cells (arrowheads) are concentrated laterally and no stained cells are present in apical region. A single stained cell can be seen in the hyponeural region (arrow). The inset shows an absence of staining in a section of a radial nerve cord incubated with antiserum that was pre-absorbed with the ArCRH peptide antigen, demonstrating the specificity of immunostaining observed in sections incubated with the antiserum. The boxed regions are displayed at high magnification in (c) and (d). (c) Immunostained bipolar-shaped cells in the ectoneural epithelium with stained processes (arrowheads) projecting into the underlying stained neuropile (*). (d) Immunostained cell in the hyponeural region and immunostained axon profiles in the neuropile of the adjacent ectoneural region. (e) Immunostaining at the junction between a radial nerve cord and an adjacent tube foot. Immunostained processes (arrowhead) appear to project from the ectoneural neuropile of the radial nerve cord into the basiepithelial nerve plexus of the tube foot. Immunostained processes (arrow) derived from the hyponeural region project around the margin of the perihemal canal. (f) Immunostaining in the marginal nerve and in the basiepithelial nerve plexus (arrowheads) of an adjacent tube foot. Immunostained processes (arrow) can also be seen here in the muscle layer the tube foot. (g) Immunostaining in a longitudinal section of the circumoral nerve ring showing immunostained cells in ectoneural epithelium (arrowheads) and immunostained processes in the underlying ectoneural neuropile (asterisk) and in the hyponeural region (arrows). Abbreviations: CONR, circumoral nerve ring; Ec, ectoneural region of radial nerve cord; Es, esophagus; Hy, hyponeural region of radial nerve cord; MN, marginal nerve; RHS, radial hemal strand; RNC, radial nerve cord; TF, tube foot; Scale bar: 250 µm in a and f; 100 µm in b and e; 25 µm in g; 50 µm in (b) inset; 12.5 µm in c and d.

Fig. 6. Immunohistochemical localization of ArCRH in tube feet of *Asterias rubens*. (a) Transverse section of an arm showing the presence of immunostaining in the radial nerve cord and adjacent tube feet. The boxed areas are shown at higher magnification in (b) and (c). (b) Immunostaining (arrow) in the sub-epithelial nerve plexus in the stem of a tube foot. Immunostained fibres (arrowhead) can also be seen here in the muscle layer. (c) Immunostaining in the basal nerve ring of a tube foot disk. (d) Immunostaining in the ampulla of a tube foot. The boxed region is shown at higher magnification in (e), which shows that the immunostaining is present in fibres located beneath the coelomic lining of the ampulla (arrowhead) and in fibres located in the muscle layer (arrow). Abbreviations: Amp, ampulla; BNR, basal nerve ring; ML, muscle layer; OS, ossicle; RNC, radial nerve cord; TF, tube foot. Scale bar: 250 µm in a; 100 µm in d; 50 µm in c; 25 µm in b and e.

Fig. 7. Immunohistochemical localization of ArCRH in the peristomial membrane, esophagus and cardiac stomach of *Asterias rubens*. (a) Transverse section of the central disk region showing immunostaining in circumoral nerve ring and peristomial membrane. The boxed region is displayed at higher magnification in (b), which shows an immunostained cell (arrowhead) in the external epithelium of the peristomial membrane and immunostained fibres in the underlying basiepithelial nerve plexus and an immunostained cell (arrow) beneath the coelomic epithelium and immunostained fibres in the underlying nerve plexus. (c) Horizontal section of the central disk region in a small juvenile specimen showing immunostained fibres in nerve plexi of the peristomial membrane and the esophagus. (d) Transverse section of the central disk region showing immunostaining in both

the cardiac stomach and pyloric stomach. Note that there is variation in the density of immunostaining in the basiepithelial nerve plexus in the folds of the cardiac stomach wall, as exemplified by the two boxed areas that are shown at high magnification in (e) and (f). (e) Region of the cardiac stomach wall adjacent to an intrinsic retractor strand; here a stained bipolar cell can be seen in the mucosal wall and the basiepithelial nerve plexus is intensely stained (********). Immunostained fibres can also be seen in an intrinsic retractor strand. (f) Region of the cardiac stomach where staining of the basiepithelial nerve plexus is less intense (…….) than in the adjacent region shown in (e). (g) Horizontal section of the central disk region of a juvenile starfish showing immunostaining in the cardiac stomach. The boxed region is displayed at higher magnification in (h), which shows variation in the intensity of immunostaining, with a region adjacent to sites of attachment of extrinsic retractor strands containing stained cells and a thickened and intensely stained basi-epithelial nerve plexus (********), whilst a neighbouring region is largely void of immunostaining (……..). Abbreviations: BNP, basi-epithelial nerve plexus; CS, cardiac stomach; CONR, circumoral nerve ring; CE, coelomic epithelium; CT, collagenous tissue; Es, esophagus; ERS, extrinsic retractor strand; IRS, intrinsic retractor strand; Lu, lumen; Mu, mucosa; PM, peristomial membrane; PS, pyloric stomach; RNC, radial nerve cord. Scale bar: 250 µm in a; 200 µm in d and g; 25 µm in e, f and h; 12.5 µm in b and c.

Fig. 8. Immunohistochemical localization of ArCRH in the pyloric stomach, pyloric ducts, pyloric caeca and rectum of *Asterias rubens*. (a) Horizontal section of a juvenile specimen showing the presence of immunostaining in the pyloric stomach, pyloric ducts and pyloric caeca. High magnification images of the boxed regions are shown in b-d. (b, c) Immunostained cells (arrowheads) in the mucosa of the pyloric stomach and pyloric duct with associated immunostained fibres in the underlying basiepithelial nerve plexus. (d) Immunostaining in the basiepithelial nerve plexus of a pyloric caecum diverticulum. (e) Transverse section of the central disk region showing immunostaining in the pyloric stomach. A high magnification image of the boxed region is displayed in panel (g), which shows intensely immunostained fibres in the basiepithelial nerve plexus. (f) Transverse sections of a pyloric duct and a pyloric caecum diverticulum showing immunostained fibres in the basiepithelial nerve plexus; note that the staining in the pyloric duct is more prominent on the oral (lower) side, as shown at higher magnification in panel (h). (i) High magnification image of the boxed region in (f), showing immunostaining in the basiepithelial nerve plexus of a pyloric caecum diverticulum. (j) Transverse section of the central disk region showing that immunostaining is present in the intestine and rectum but not in the rectal caeca, which emanate at the junction of the intestine and rectum. High magnification images of the boxed regions are displayed in (k) and (l). (k) Junction between the rectum and the anal opening in the aboral body wall of the central disk; note the intense staining in the nerve plexus (arrows) beneath the coelomic epithelium of the rectum. (l) Immunostaining in both the visceral muscle layer (arrowhead) and sub-mucosal basiepithelial nerve plexus (arrow) of the intestine. Abbreviations: An, anus; BNP, basiepithelial nerve plexus; CS, cardiac stomach; Ce, coelomic epithelium; In, intestine; Lu, lumen; Mu, mucosa; PC, pyloric caecum; PD, pyloric duct; PS, pyloric stomach; RC, rectal caecum; Re, rectum. Scale bar: 250 µm in a and f; 200 µm in e and j; 50 µm in g, h, I, k and l; 25 µm in b, c and d.

Fig. 9. Immunohistochemical localization of ArCRH in body wall-associated structures in *Asterias rubens*. (a) Transverse section of an arm showing immunostaining in the apical muscle and an adjacent papula. High magnification image of the boxed region is shown in (b). (b) An immunostained cell (black arrowhead) can be seen in the coelomic lining of the apical muscle and profiles of immunostained fibres (arrows) are amongst the longitudinally orientated muscle fibres of the apical muscle. Immunostained fibres can also be seen here in the circular muscle layer of the body wall (white arrowhead). (c) Transverse section of an arm showing the presence of immunostaining in the nerve plexus beneath the coelomic epithelial lining of a papula (black arrowheads), which is contiguous with the basiepithelial nerve plexus of the epithelium lining the main coelomic cavity of the arm. Immunostaining can also be seen here in fibres (white arrowheads) that are contiguous with the nerve plexus associated with the circular muscle layer of the body wall. (d) Immunostaining in the sub-epithelial nerve plexus (arrows) beneath the external epithelium of the aboral body wall. Abbreviations: CMLNP, circular muscle layer nerve plexus; CBNP, coelomic basiepithelial nerve plexus; CT, collagenous tissue; Pa, papula; SNP, sub-epithelial nerve plexus. Scale bar: 100 µm in a, c and d; 25 µm in b.

a

MNDLQRLILLVSLGTFALLLCLPACTEAQPLGLFKFEYDDLLDPSFEADDPRNPR
RLSRQQILRRLNDLAMSRSGSGPGYTIPRKRQGLSVSPIFPIQRIRLNAIERDRQ
DQVDQAEANQGLFQIAGRKR

b

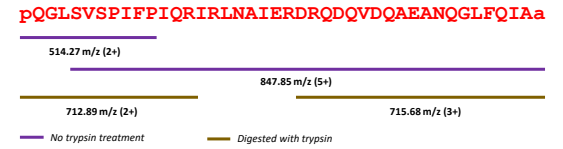

c

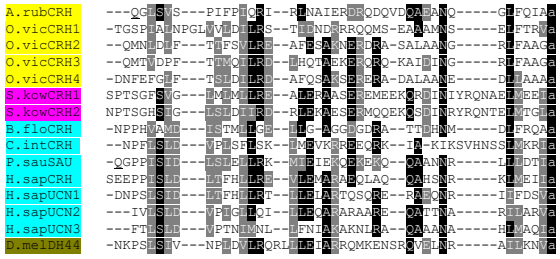

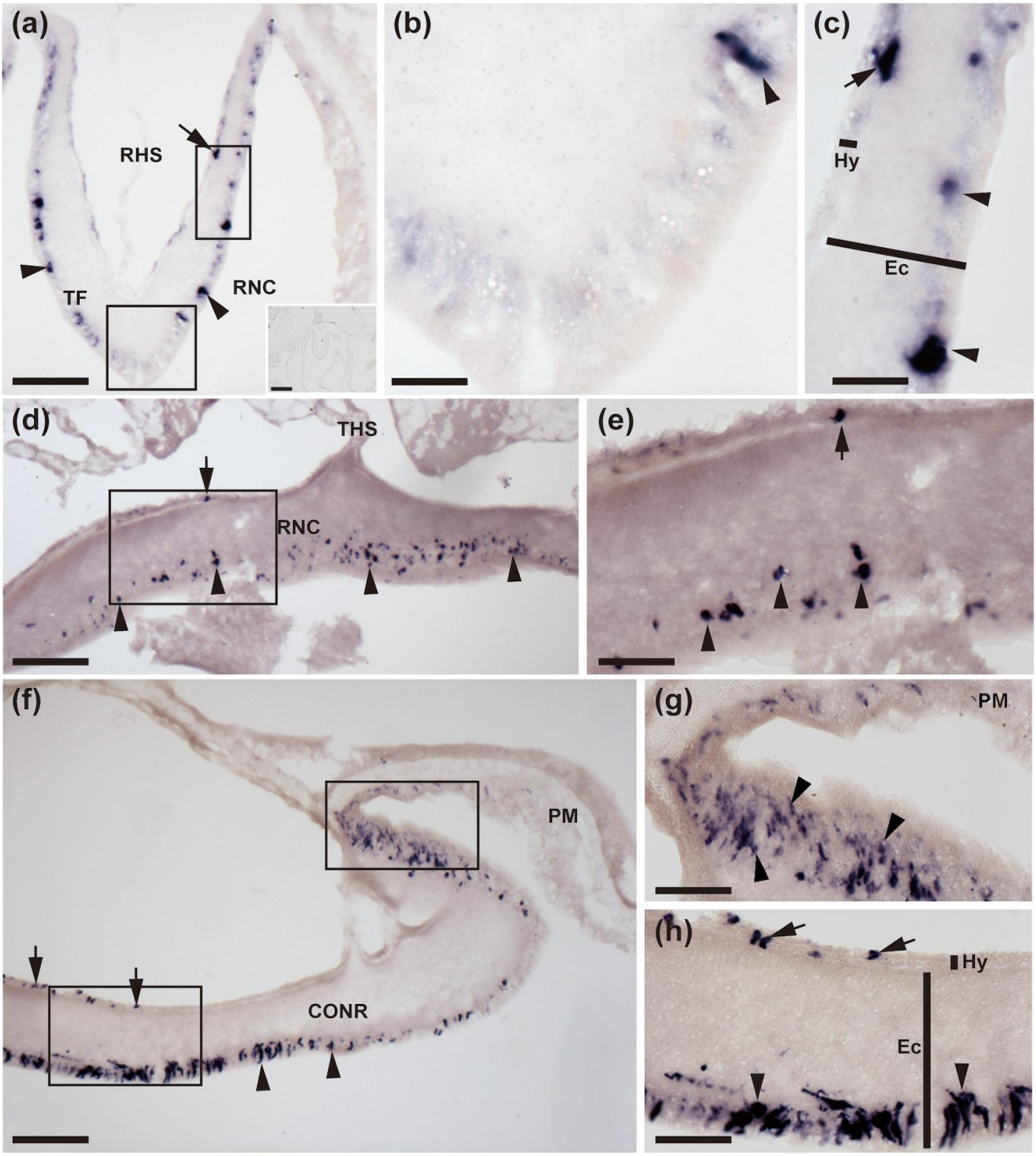
(a)
RHS
TF
RNC
(b)
(c)
Hy
Ec
(d)
THS
RNC
(e)
(f)
PM
CONR
(g)
PM
(h)
Hy
Ec

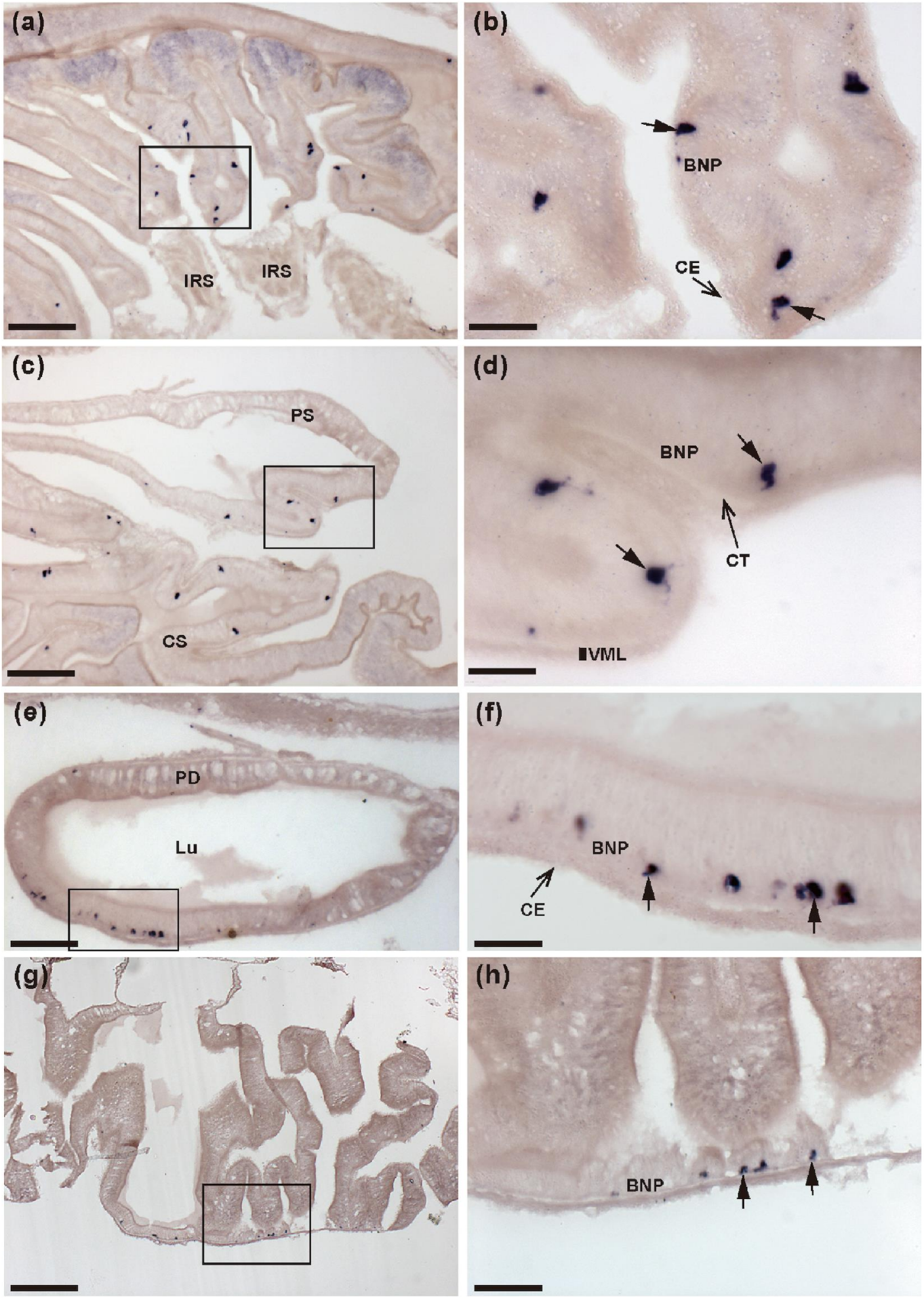
(a)
IRS
IRS
(b)
BNP
CE
(c)
PS
CS
(d)
BNP
CT
VML
(e)
PD
Lu
(f)
BNP
CE
(g)
(h)
BNP

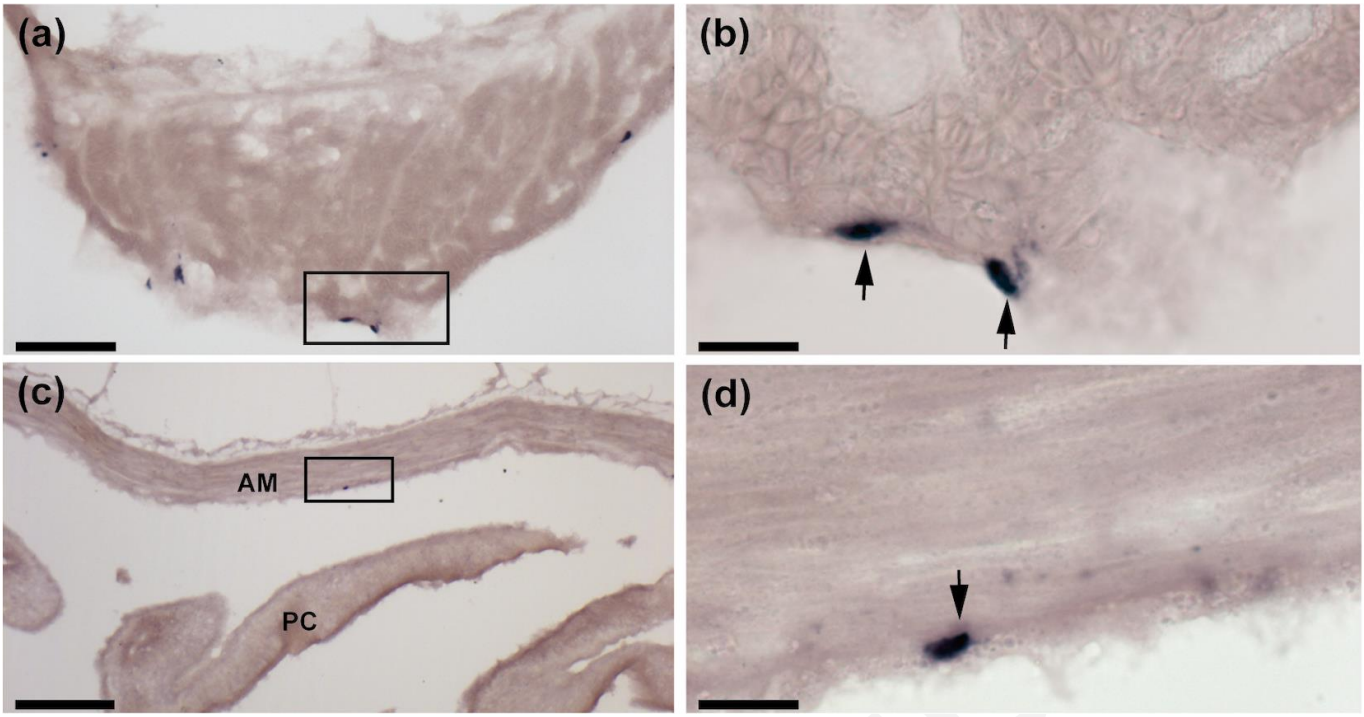

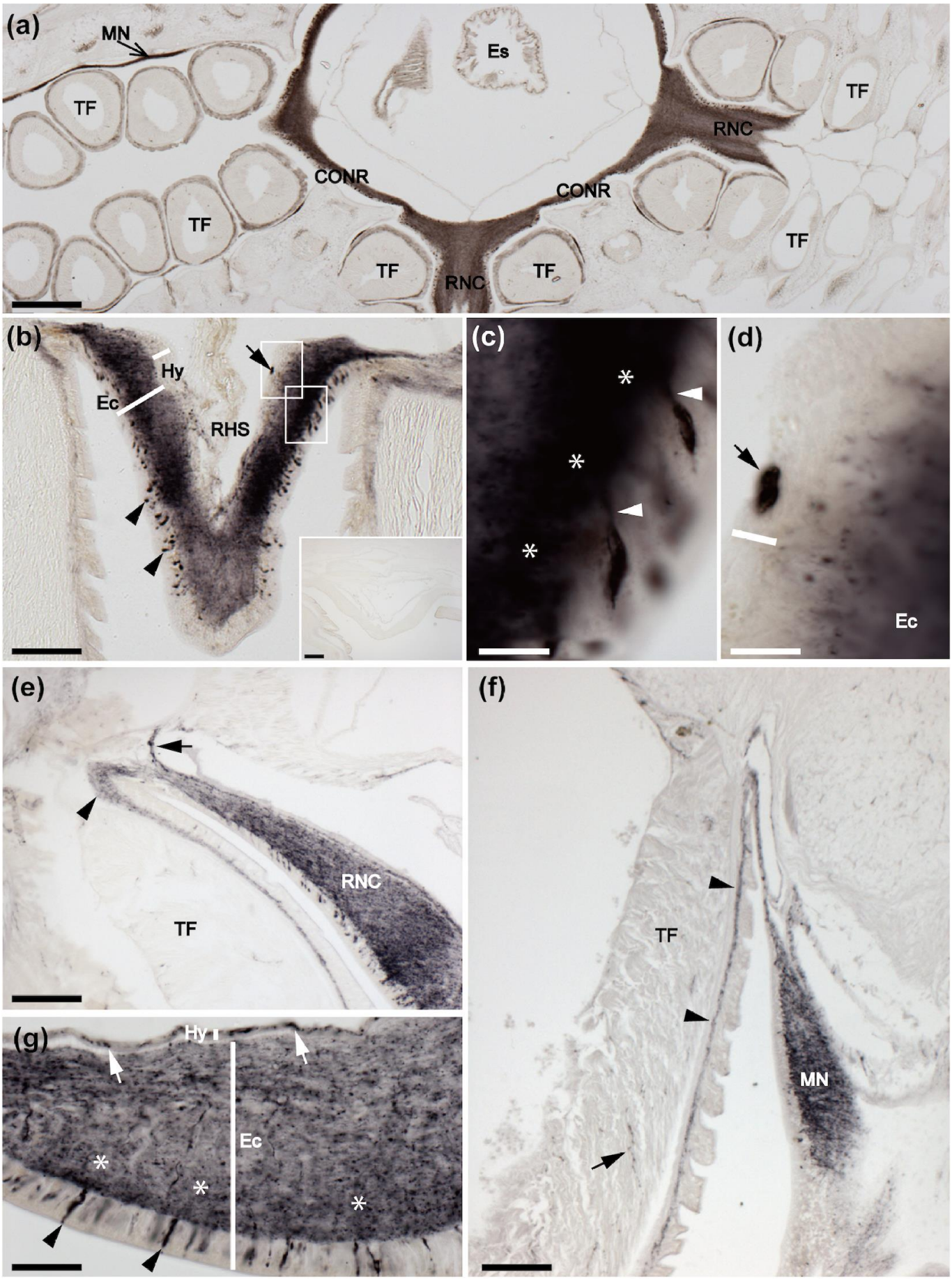
(a)
MN
Es
TF
TF
RNC
CONR
CONR
TF
TF
TF
TF
RNC
TF
(b)
Hy
Ec
RHS
(c)
(d)
Ec
(e)
RNC
TF
(f)
TF
MN
(g)
Hy
Ec

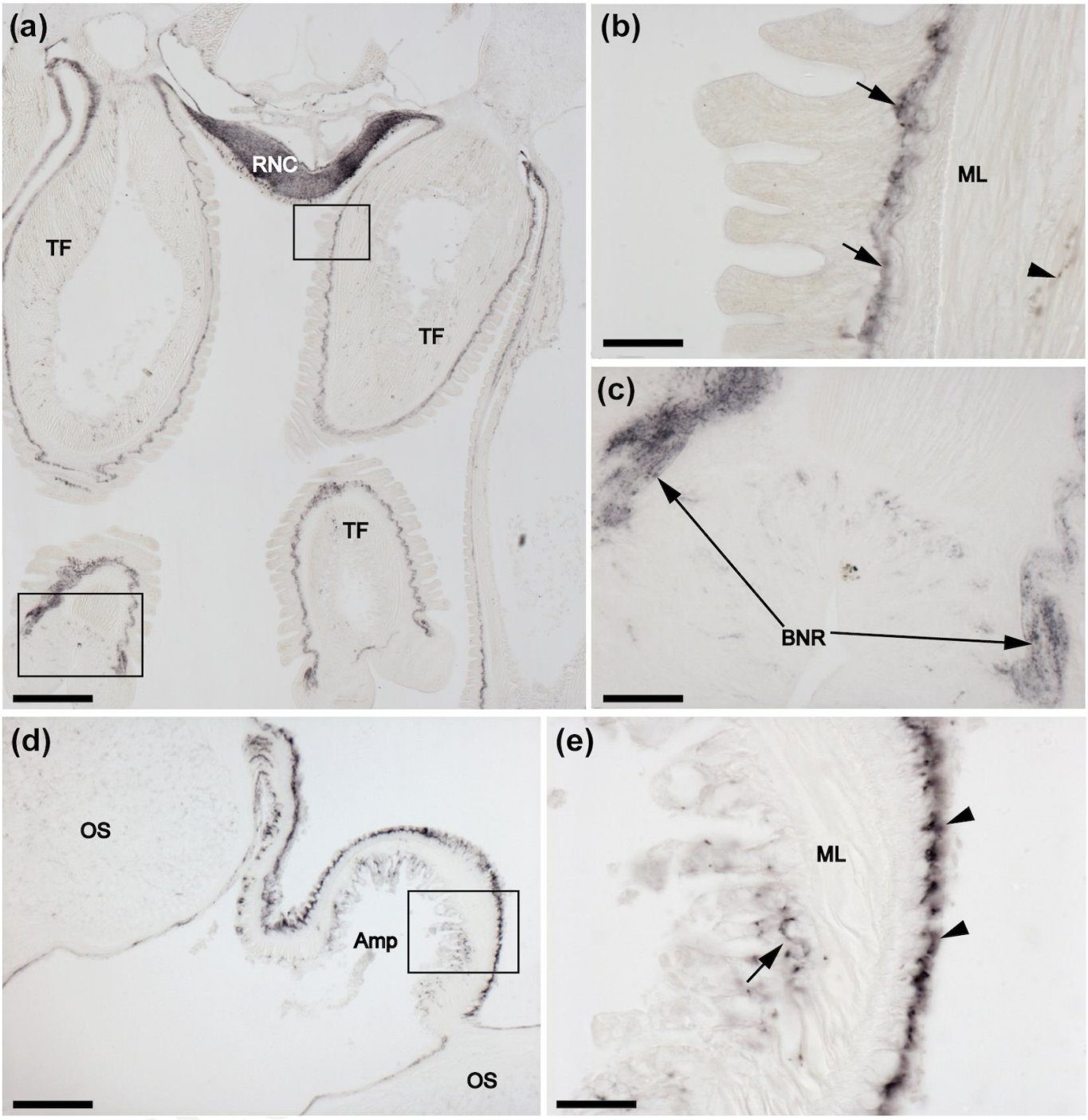
(a)
RNC
TF
TF
TF
(b)
ML
(c)
BNR
(d)
OS
Amp
OS
(e)
ML

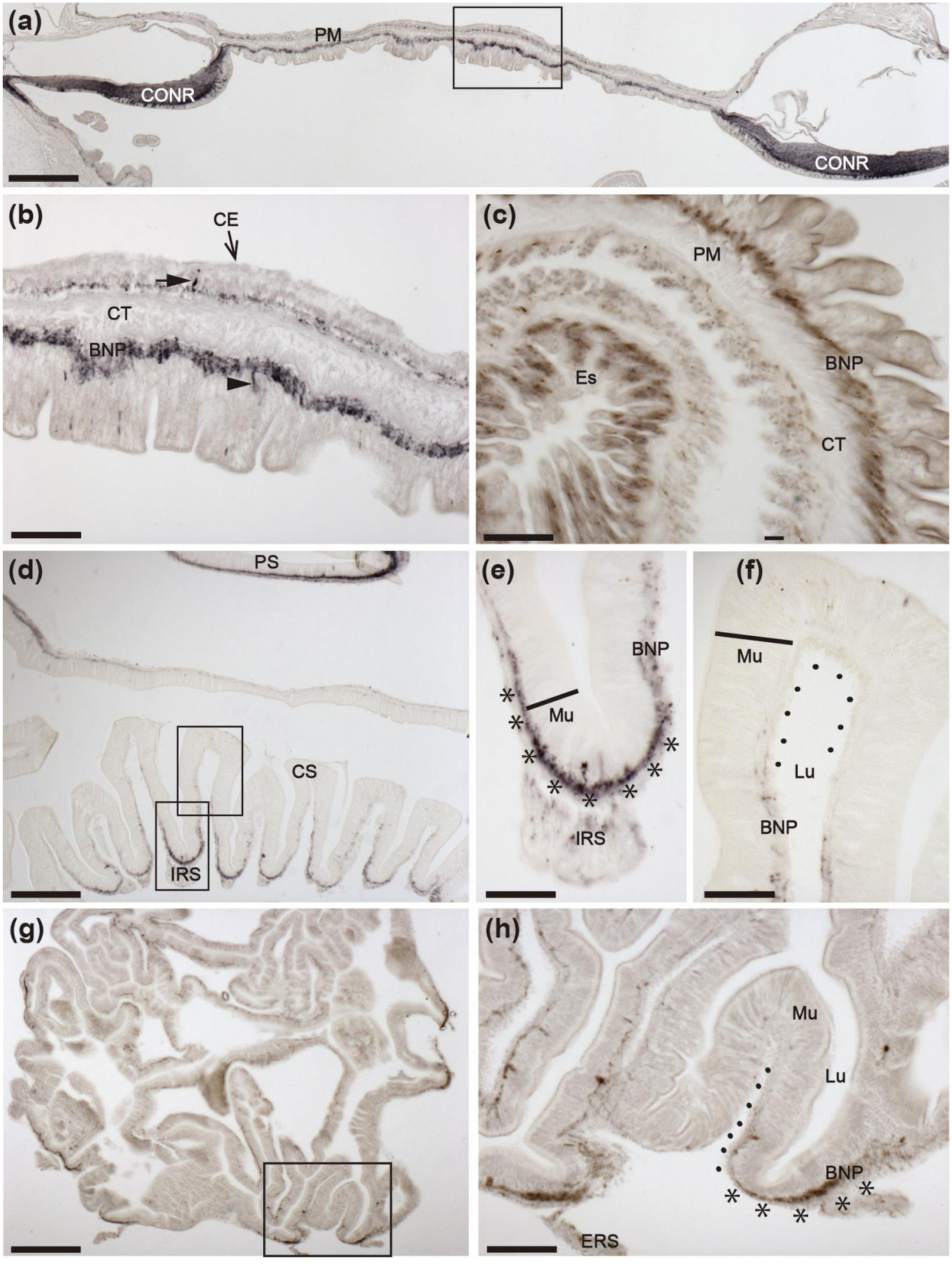
(a)
PM
CONR
CONR
(b)
CE
CT
BNP
(c)
PM
Es
BNP
CT
(d)
PS
CS
IRS
(e)
BNP
Mu
IRS
(f)
Mu
Lu
BNP
(g)
(h)
Mu
Lu
BNP
ERS

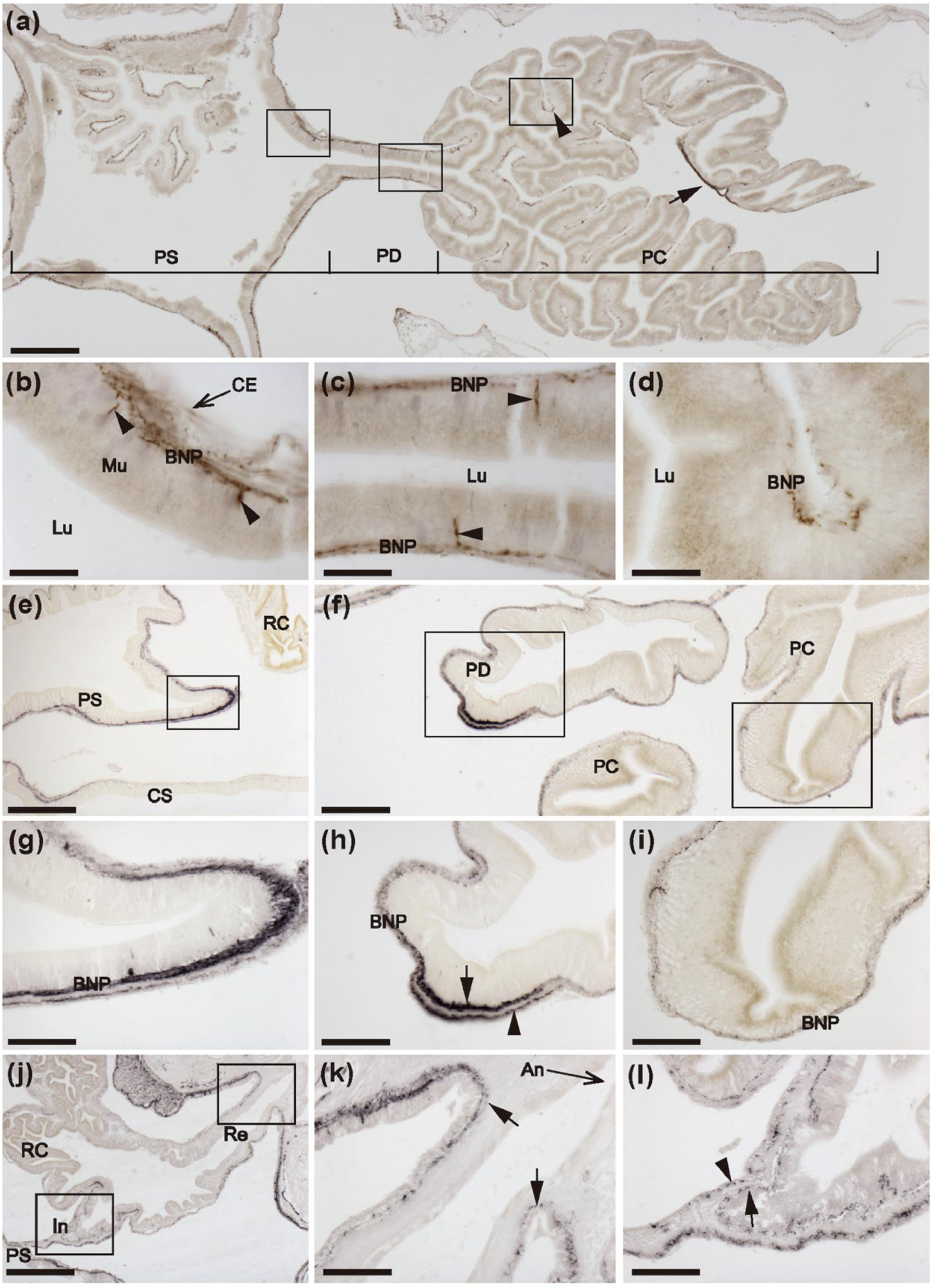
(a)
PS
PD
PC
(b)
CE
Mu
BNP
Lu
(c)
BNP
Lu
BNP
(d)
Lu
BNP
(e)
RC
PS
CS
(f)
PD
PC
PC
(g)
BNP
(h)
BNP
(i)
BNP
(j)
Re
RC
In
PS
(k)
An
(l)